Paper:

Experimental Study on Flexural Behavior of Reinforced Concrete Walls

Sergio Sunley[*1], **Koichi Kusunoki**[*2], **Taiki Saito**[*3], **and Carlos Zavala**[*4]

[*1]Universidad Centroamericana José Simeón Cañas (UCA)
PO 01-168, San Salvador, El Salvador, Centro América
E-mail: Sunley612s@Gmail.com
[*2]Yokohama National University
79-5 Tokiwadai, Hodogaya ku, Yokohama City, Kanagawa 240-8501, Japan
[*3]Department of Architecture and Civil Engineering, Toyohashi University of Technology
1-1 Hibarigaoka, Tempaku-cho, Toyohashi 441-8580, Japan
[*4]Faculty of Civil Engineering, CISMID, National University of Engineering (UNI)
Av. Tupac Amaru, 1150 Rimac, Lima 25, Peru
[Received November 5, 2012; accepted January 8, 2013]

Design codes prescribe equations for the ultimate state design of RC walls with flange walls as boundary elements. These codes consider part of the length of the flange wall as a width that will effectively resist lateral loads. However, wall damage and the accuracy of the effective width used in the calculations have not been sufficiently discussed. Therefore, a loading test is carried out at Yokohama National University on two 1/3 scale specimens in order to evaluate the strength, damage, energy dissipation, and behavior of RC structural walls in flexure. One specimen without flange walls and one with flange walls are tested. The strength and response of each specimen are described, and the prediction accuracy of the design flexural strengths given by design codes ACI, Eurocode, and AIJ are examined. Experimental strain data are used to describe the behavior of the flange wall in order to understand the mechanism and to confirm the accuracy of the effective width prescribed by the design codes in terms of tension and compression. The result of the experimental study reveals that design prescriptions given by ACI, Eurocode, and AIJ guidelines can conservatively estimate the flexural strength for RC walls without flanges, but they underestimate the flexural strength for flanged walls. This underestimation is due to a lack of knowledge of the mechanism that develops at the flange. It is not possible to determine a specific value for flexural effective width. However, according to the results of calculations, a portion larger than the width proposed by the aforementioned design codes serves to resist the stresses imposed by lateral loads. Therefore, it is confirmed that the flange width is underestimated by the design codes, and it increases with the imposed drift level. The stress distribution at the flange in the out-of-plane direction is found not to be uniform, a fact that is at odds with design assumptions.

Keywords: flange wall, effective width, flexural strength

1. Introduction

The use of reinforced concrete walls as a structural element to resist the lateral loads imposed by earthquakes is common in countries prone to strong ground motion seismicity. Generally, reinforced concrete walls are called shear walls because they commonly resist the lateral load as a shear behavior element prior to flexural behavior. When flange walls are attached to structural walls (web-walls), they contribute to lateral resistance. The 2010 earthquake in Chile provided evidence of the importance of enhancing the knowledge and design for the flexural behavior of RC walls was. Damage was caused to several different buildings where the main resistance system consisted of RC walls without frames [1]. The main objective of this study is to acquire knowledge of the behavior of RC walls in flexure and of the mechanism the flange walls develop in particular. This is accomplished by analyzing the experimental results of cyclic loading tests conducted in Yokohama National University.

2. Concept

When boundary elements of shear walls are RC walls, practice consists of considering the plane wall section as a beam with flanges. In this case, the length of the flange wall that resists part of the moment caused by lateral load is called the effective width (**Fig. 1**). It is possible to define the effective width according to the stress distribution in the flange wall if it is considered that the stress distributes, as shown in **Fig. 1**. For a given stress σ_t, which is highest at the in-plane wall and decreases with the distance from the center of the flange wall, the total force in the flange walls F can be calculated as the integral of the tensile stress for tension or compression stress independently.

The effective width "B" is given by Eq. (1), where t is the thickness of the web wall, which is the same for both

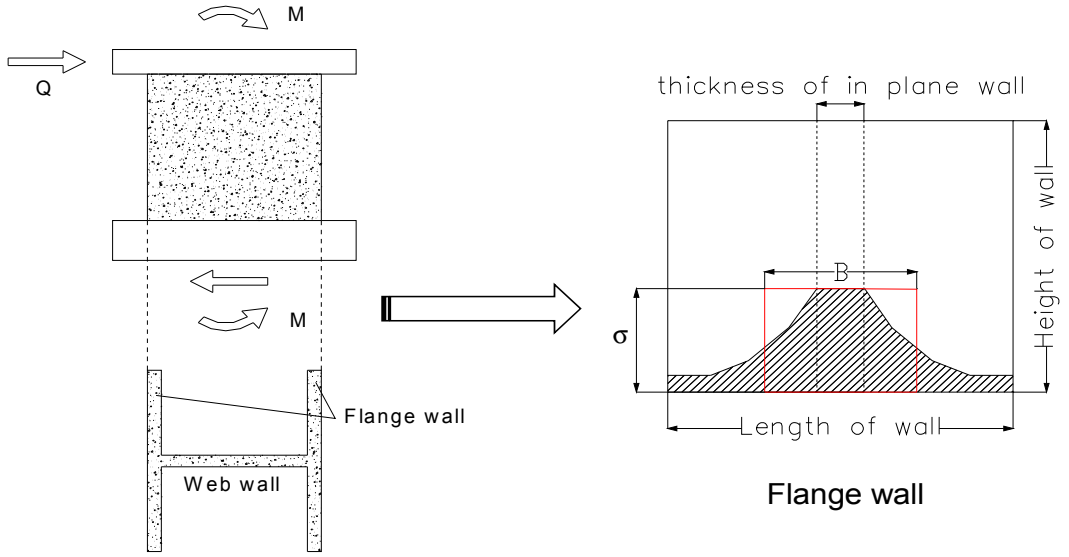

Fig. 1. Stress distribution for flange walls assumed in the experimental test.

the web and flange walls in the experiment.

$$\sigma_t \times B \times t = F \quad \ldots\ldots\ldots\ldots\ldots\ldots \quad (1)$$

The AIJ [2] guideline uses Eq. (2) for the calculation of flexural strength. ACI [3] and Eurocode [4] use a linear strain distribution using the concept of stress compression block at the concrete.

$$_W M_u = a_t \cdot \sigma_{sy} \cdot l_W + 0.5 \sum (a_{wy} \cdot \sigma_{wy}) \cdot l_W + 0.5N \cdot l_W \quad \ldots\ldots\ldots\ldots\ldots\ldots \quad (2)$$

where

N: Total axial force in the boundary elements attached to the wall

a_t: Cross sectional area of the flexural reinforcement bars of a boundary element

$\sum a_{wy}$: Cross sectional area of the flexural reinforcement bars in the wall

σ_{sy}: Yield strength of the flexural reinforcement bars of a boundary element

σ_{wy}: Yield strength of the flexural reinforcement bars in the wall

l_w: Distance between the centers of the boundary columns of the wall

3. Test

A cyclic static loading test was conducted at Yokohama National University with 1/3 scale specimens in order to evaluate the flexural behavior of structural walls with walls as boundary elements. For this purpose, no axial load was applied. The behavior of two specimens is discussed: N1 and N2. Specimen configuration targets a middle-height reinforced concrete wall structure, and it was intentionally designed to fail in flexure prior to shear failure according to the provisions of the AIJ Guidelines.

Table 1. Dimensions and reinforcement arrangement.

Description		Steel reinforcement				
		Thickness	Vertical	Horizontal	At ends	Pwe (%)
N1	In-plane	80 mm	2-D4@150	2-D5@150	2-D5	0.37
N2	In-plane	80 mm	2-D4@150	2-D5@150	2-D5	0.24
	Flange					

Table 2. Material properties.

Concrete Properties	**Young Modulus (MPa)**	**Tensile Stress (MPa)**	**Ultimate Stress (Mpa)**
N1	2.54×10^4	2.48	31
N2	2.53×10^4	2.26	31
Steel Properties (SD295)	**Young Modulus (MPa)**	**Yielding Stress (MPa)**	**Ultimate Stress (Mpa)**
D4	1.85×10^5	356	505.8
D5	1.92×10^5	364	524.4

3.1. Overview of the Specimens

The specimen N1 was a wall without flange walls at the ends, and specimen N2 was a wall with flange walls at both ends in plane. They were designed taking into account the effective width of the walls, which is 6 times the thickness of the central wall for each wing wall, as prescribed by AIJ Guidelines [2]. The reinforcement description and material properties for the concrete and steel are summarized in **Tables 1** and **2**, respectively. A plain view of each specimen is shown in **Figs. 2** and **3**.

3.2. Load System

Cyclic reversal lateral loading was applied statically to each specimen through one 1MN hydraulic jack. The load

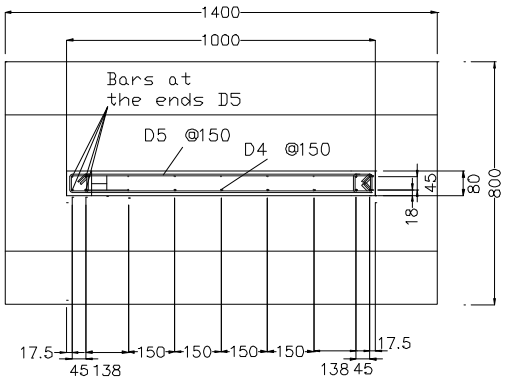

Fig. 2. Plan view specimen N1.

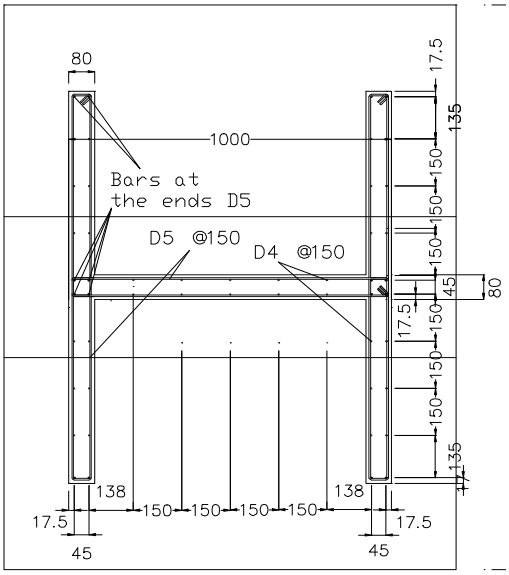

Fig. 3. Plan view specimen N2.

was transmitted by a rigid beam at the top of the wall and controlled by displacement at the same level. Two 200 kN hydraulic jacks kept the vertical load at zero, so that the wall did not carry axial load (see **Fig. 4**). The lateral load was transmitted to the wall by the anchorage of the beam at the top of the wall.

The loading protocol consisted of the following drift target angles: $\pm 1/6400$ (0.016%), $\pm 1/3200$ (0.03%), $\pm 1/1600$ (0.0625%), $\pm 1/800$ (0.125%), $\pm 1/400$ (0.25%), $\pm 1/200$ (0.50%), $\pm 1/100$ (1%), $\pm 1/66$ (1.52%), $\pm 1/50$ (2%), and $\pm 1/25$ (4%). The positive direction was push toward the south. After $\pm 1/800$, each cycle was repeated once.

4. Experimental Results and Analysis

4.1. Specimen N1

The first crack was observed at the drift angle of $+1/3200$ ($R = +1/3200$) at the lower north corner of the wall. This horizontal crack was a clear pattern of flexural

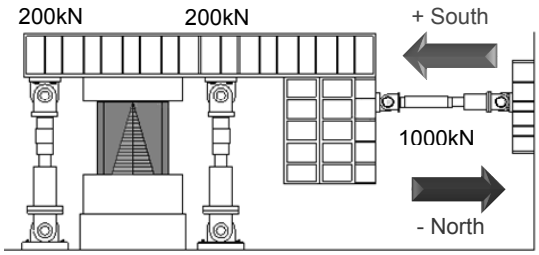

Fig. 4. Loading system.

behavior expected at the wall. The same crack was observed on the south side when the load was reversed to the opposite direction. At $R = +1/1600$, diagonal cracks appeared at the lower north corner. The same pattern of diagonal cracks at the bottom of the wall developed in the following cycles in both directions, with new ones appearing up the height of the wall. Important cracks were measured from drift angle $R = -1/800$, at which the maximum crack width was 0.3 mm (at crack a in **Fig. 5a**). The first reinforcement bar yielded on the north side at $R = +1/800$, and at $R = \pm 1/400$, all the bars at the corners of the bottom of the wall yielded at load 58.6 kN f and 52 kN for the positive and negative direction, respectively. The maximum load was observed at $R = \pm 1/200$, and it was 67 kN for the positive direction and 71 kN for the negative direction. In the same cycle, the cracks A and b in **Fig. 5a** opened 0.95 mm and 1.50 mm, respectively. After this drift angle, the same crack pattern continued with consequent growing of cracks. At $R = \pm 1/100$, sliding of the base of the wall occurred. At $R = \pm 1/50$, compression failure was observed for the concrete in the lower corners with steel buckling; cracks B and b opened 5 mm and 4.5 mm, respectively. The wall resistance decreased slightly, exhibiting ductile behavior. The specimen lost carrying capacity at $R = 2.5\%$, which was evidenced by a decrease in the restoring force with the displacement increment, as shown in **Fig. 6a**. The test continued until $R = +4.48\%$, when it was stopped because of equipment limitations. In the last stage, cracks A and a opened completely.

4.2. Specimen, N2

Figure 7 is a plan view of specimen N2. It is included so that the crack propagation pattern presented for that specimen may be understood.

In this test, small cracks were observed at $R = +1/6400$ on the south side at the intersection of the web and flange walls. At $R = +1/1600$, a horizontal crack appeared at the base of the north flange, and a similar crack developed at the base of the south flange at $R = -1/1600$. The maximum load of 150 kN occurred just before reaching the drift angle of $R = +1/800$, followed by the sudden formation of diagonal crack A1 in **Fig. 5b**. Crack A1 extended from the upper north corner to the lower south corner of the wall and the restoring force sudden decreased.

The diagonal crack at this drift also extended to the north flange, and it measured 0.85 mm in width at the rep-

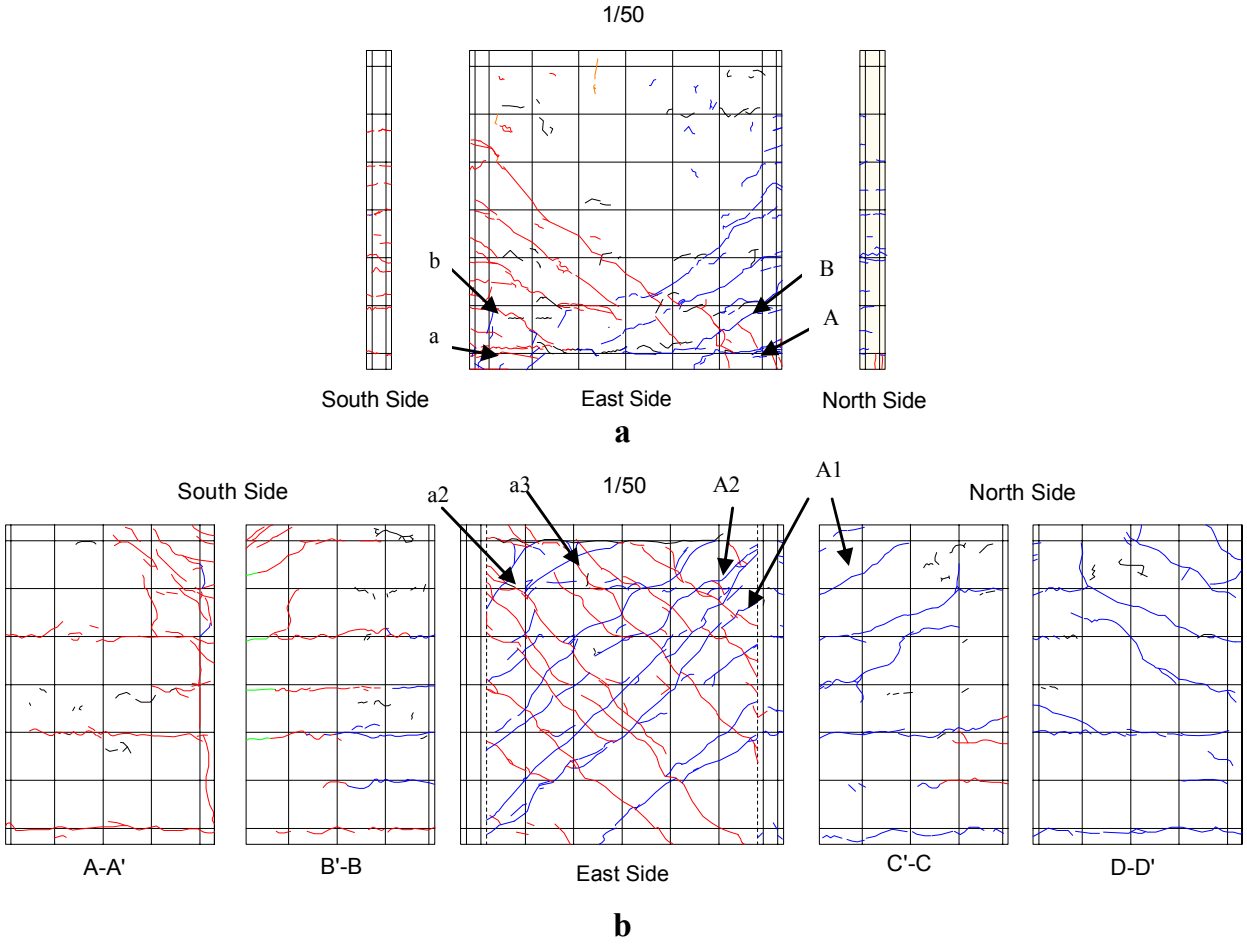

Fig. 5. Crack pattern for specimen N1 and N2 at the stage of drift angle 1/50 presented for the experimental test.[1]

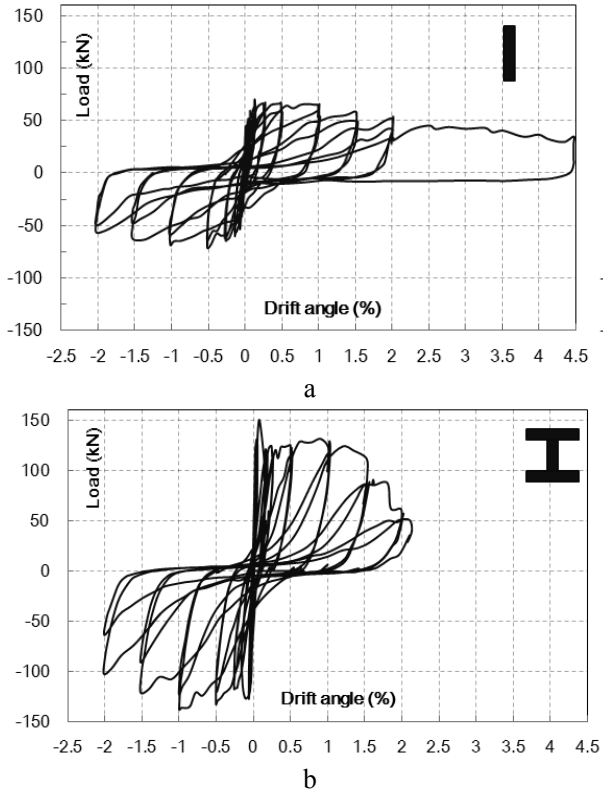

Fig. 6. Load vs. Drift curve from experimental test. a is specimen N1, b is specimen N2.

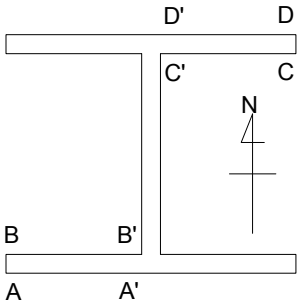

Fig. 7. Scheme of specimen N2, plan view.

etition of the loading cycle. After this stage of the test, important cracks were measured until the end of the loading protocol. Several diagonal cracks were developed after a drift of $R = 1/400$ in both directions, and those cracks were also extended to the flange walls. At $R = +1/100$, the vertical reinforcement bars started to yield at the base of the corner of each side at a load of 124 kN. However, the cracks close to those bars opened less than 0.45 mm. In the same stage, diagonal cracks A1 and A2 in **Fig. 5b** measured, 3.5 mm and 5 mm, respectively, at the positive peak, and cracks a2 and a3 measured 6 mm and 2.50 mm,

1. Blue cracks appeared when the load towards to the south and red cracks appeared when the force goes toward to north.

respectively, at the negative peak. At $R = 1.20\%$, (at cycle $R = +1/66$), most of the bars of the specimen yielded. After this step, the wall decreased its carrying capacity. The wider crack opening was observed at the repetition of the load at the drift $R = \pm 1/50$, and it was 18 mm for crack A2 and 8 mm for crack a2. The test stopped at $R = 2.10\%$ because tensile failure of the vertical reinforcement bars occurred at the top of the north corner of the wall. This is attributed to the loading system, which consisted of a rigid beam, causing stresses to be concentrated around the zone fixed to the wall. No compression failure of the concrete was observed during the test. After $R = \pm 1/66$, wall resistance suddenly decreased, presenting brittle behavior (**Fig. 6b**).

Figure 8 shows the comparison of skeleton curves for N1 and N2.

4.3. Energy Dissipation Capacity

The energy dissipated by the inelastic behavior of specimens is described by the area enclosed inside hysteresis loops [7]. The energy of deformation is calculated for each specimen as the mentioned area at each step, as shown in **Fig. 9**.

4.4. Evaluation of the Predicted Behavior

An assessment of the prediction accuracy of flexural strength based on the design methods mentioned in section 2 was made. For this purpose, the flexural design strength for each specimen was calculated and compared with the skeleton curve resulting from each specimen tested.

The calculation methods used to estimate the flexural strength were: JBDPA-AIJ [2], ACI 318-08 [3], and Eurocode2 (2004) [4]. Three cases are presented:

- Flexural strength for specimen N1
- Flexural strength for specimen N2, using the proposed effective width of each design code.
- Flexural strength for specimen N2, considering the complete flange as the effective width.

Material test results were used for the calculations. The maximum compression strain of the concrete was taken as the strain corresponding to the maximum load of the concrete compression test. The behavior of the steel was assumed as perfect elastic plastic for the calculation of the strength, according to [2] and [3].

Moreover, two additional values were compared: the force corresponding to 80% of the maximum load test and the load corresponding to the point where most of the bars were observed to yield.

Eighty percent of the maximum load is an empirical value that is commonly used to estimate the ultimate limit state of cyclic-tested RC elements. The load corresponding to the flexural strength and the other values mentioned are presented in **Tables 3** and **4**.

It was found in the comparison that, for specimen N1, the prediction of the three design codes was almost the same, as was the value corresponding to 80% of the maximum load. But even if the design equations considered the yield of all bars at the moment of maximum strength load, the specimen presented more strength than that indicated by the calculations. It can be said that the design assumptions describe in an acceptable manner the flexural failure, because the specimen showed that compression failure of the concrete and the yielding of the vertical reinforcement bars gave conservative results. It is important to mention that the equations do not consider the cyclic behavior of the element.

For specimen N2, design equations of the ACI and Eurocode gave almost the same value for flexural maximum strength as a consequence of using the same model with only small modifications in the parameters. This value was smaller than the one calculated with the AIJ prescription. The three values were smaller than the point at which the bars yielded in the test. Here it is important to take into account the different considerations of each design code. First, AIJ uses an effective width of the flange wall for flexure of 6 times the thickness of the wall, which is 480 mm per wing wall. For the calculation with ACI and Eurocode, the effective width used was 25% of the height of the wall extended from the face of the web wall. It means a total effective width of 580 mm was used for this test. Another difference is that AIJ does not consider the concrete contribution for the ultimate flexural strength.

When the calculation was performed for specimen N2 with the complete flange used as the effective width, the result for all the cases yielded a larger strength capacity. This suggests that the considered flange was longer than the prescribed one but shorter than the complete flange for this tested specimen.

5. Estimation of the Effective Width

The calculation of the effective width was performed for specimen N2, based on the basic concept presented in **Fig. 1** for both tension and compression stress conditions. If the strain history from strain gauges attached at a height of 90 mm from the bottom of the wall is used, the stress distribution can be obtained. It is with that stress, that the value of the effective width B is estimated.

Effective width at the flange is calculated by dividing the integral of the total area under the stress distribution by the value of the central stress. For the flange walls, readings from the strain gauges attached to the lowest section are taken from lines AA′, BB′, CC′, and DD′ at each peak of the load-displacement (**Fig. 7**). When compression effective width is calculated, readings taken by lines AA′ and BB′ come from the positive displacement peaks, and the readings taken for lines CC′ and DD′ come from the negative displacement peaks. The opposite convention is used for tension. For compression effective width, the stress of the concrete is calculated considering the linear behavior of the material, so the stress is given by the multiplying the strain by Young's modulus of the concrete. Only strain data from layers AA′ and DD are used in the

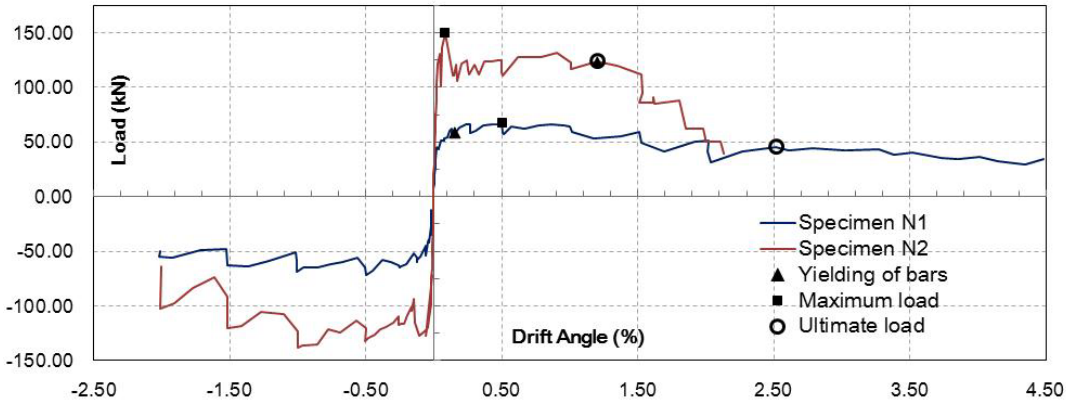

Fig. 8. Skeleton curve of specimens N1 and N2.[2]

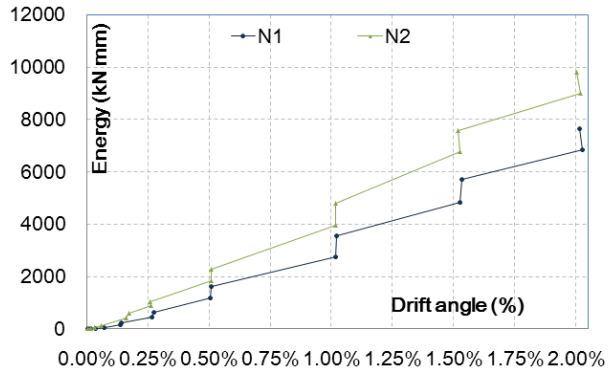

Fig. 9. Energy dissipation capacity for each specimen.

Table 3. Critical points in the skeleton curve.

Yielding of bars (kN)	Ultimate Load (kN)
65.9 (R=0.25%)	45.4 (R=2.52%)
124 (R=1.20%)	124 (R=1.20%)

Table 4. Ultimate maximum load in flexure according to design codes.[3]

Specimen	Calculated			From test
	AIJ	ACI	Euro code	80 % Max
N1	52.4 (79.6%)	54.5 (82.6%)	54.4 (82.6%)	53.9
N2	107.7 (86.8%)	76.2 (61.4%)	76.1 (61.4%)	119.9
N2 (total flange)	137.1 (110.6%)	147.5 (119.0%)	147.5 (118.9%)	

calculation of compression effective width, because it was determined that BB′ and CC′ carried tensile stress. For steel, the stress is calculated with the strain history by using the bilinear model, with Young's modulus and yielding forces as parameters for the model for all the layers.

Figures 10 and **11** show the variation in the calculated compression and tension effective width, respectively, for this tested specimen, where the total length of the wall is 1250 mm. According to the curve corresponding to line AA′ and BB′, the values of effective width resulting from the calculation are larger than the real length of the flange wall for tension and compression. This is incongruent, because it implies that the effective width is larger than the real length of the flange wall. It was determined that this result presented that trend because strains (and consequently stresses) obtained by the data acquisition system revealed that flange walls developed a strain and stress distribution in which the maximum was not always at the center of the element. This fact is not described by the concept of effective width explained in section 1. The load was applied directly to the web wall and not to the flange; therefore, the maximum strains (and stresses) were expected to develop at the intersection of the two walls.

To better understand the stress distribution in the flange zone, data acquired by the strain gauges on the concrete surface of flange walls were used to estimate the shape of the compression zone.

From the readings of the strain gauges attached to the concrete, the depth of the compression zone in plane was determined assuming a linear distribution of strain (**Fig. 12**). The calculation revealed that the tensile stress area was bigger in the intersection of flange and web wall. This is a possible reason for the presented distribution of strains and the non-applicability of the proposed method for the calculation of the effective width.

This could also indicate the possibility of local stress affecting the test results.

Another possible reason for the strain distribution obtained is that the direction of the applied load was not well aligned with the axis of the web wall. This might have caused the load not to be transmitted perpendicular to the flange wall, which would have affected the stress distribution configuration.

It is also possible that the damage was predominant at the top of the wall and not at the bottom. If damage was concentrated at the shear cracks, the wall accumulated shear deformation and did not behave as a flexural element.

2. The yielding of the bars, maximum load and ultimate load are remarked.
3. The percentage of each calculated strength value respect to the load corresponding to the maximum number of bars yielded is shown in parenthesis.

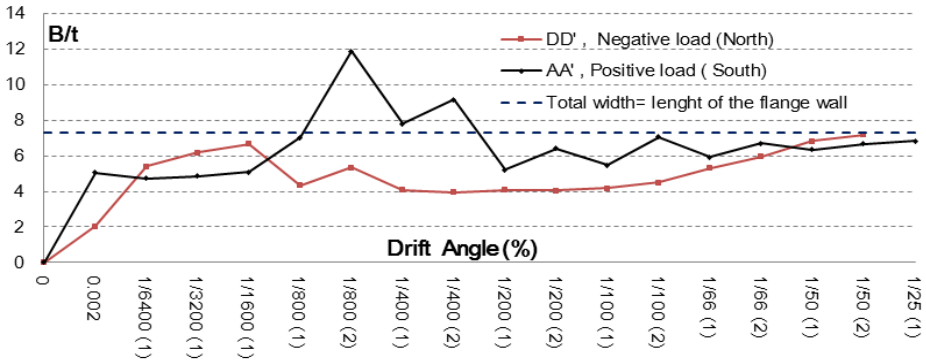

Fig. 10. Results of the calculation of effective width in compression.

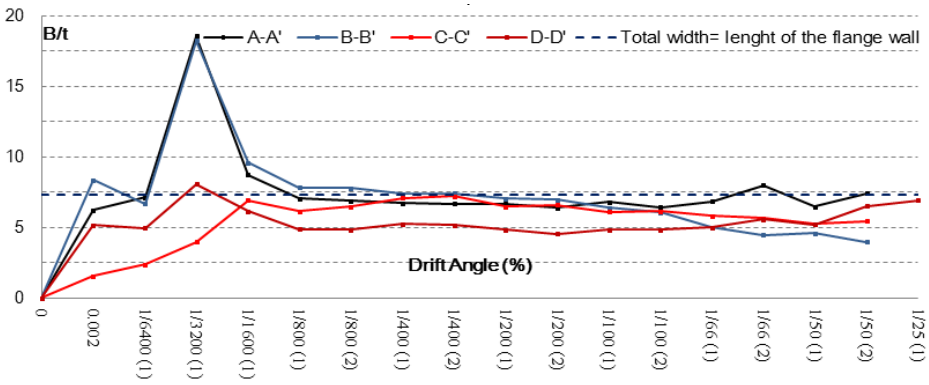

Fig. 11. Results of the calculation of effective width in tension.

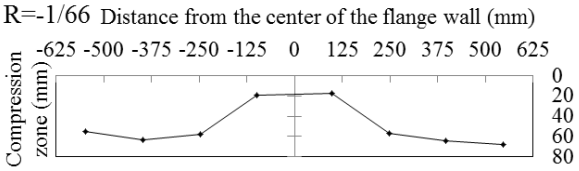

Fig. 12. Scheme of the compression distribution in flange walls.

5.1. Effective Reinforcement Ratio

It is important to know not only the effective width of the flange wall but also the amount of reinforcing steel that effectively resisted the tensile force. The total force carried by each flange was calculated using approximated stress values and then the required area of steel at each drift angle was determined.

The ratio of the sum of the stresses in the flange wall to the stress under which the bars yielded gives the equivalent number of yielded bars that resist the tensional force due to the flexural moment.

The total area of steel is found by multiplying the equivalent number of bars by the area of a selected steel bar, in this case the result is expressed in terms of the stress at which D4 bars yield.

The calculated area of steel is expressed as the reinforcement ratio (Eq. (3)) on the gross area of the wall. It means the amount of reinforcement that yielded and is necessary to resist the tensile force in the flange at each peak of the loading test (see **Fig. 13**). It can be noted from the figure that the required reinforcement ratio to resist the tensile force in the test was smaller than the reinforcement ratio provided by the whole flange.

$$\rho_e = \frac{A_S}{t \times L_f} \quad \ldots\ldots\ldots\ldots\ldots\ldots \quad (3)$$

where

ρ_S: Effective reinforcement ratio for flange walls
A_S: Equivalent required area of steel at yielding point
t: Thickness of flange wall
L_f: Length of the flange wall

One should not lose sight of the fact that the effective reinforcement ratio was calculated only based on the gross area of the flange; it did not take into account the steel bars at the web or the other flange. This is because the purpose to describe the tensile flange behavior.

According to the results, the maximum required reinforcement ratio was 0.32% at the south flange. That was also more than the corresponding value for the width *6 t*.

5.2. Observations

In order to estimate the effective width from the experimental data, strain gauges were used. However, if cracking or micro-cracking of the concrete occurred in the early stages of the test, the experimental measurements of the strain could have resulted in values that were larger than the ones corresponding to the actual stress due to the crack

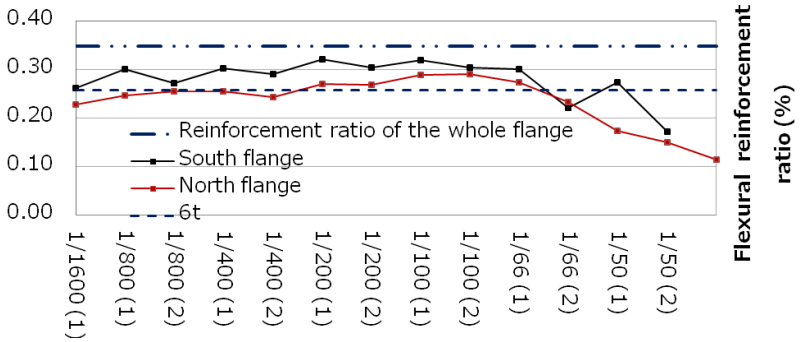

Fig. 13. Effective reinforcement ratio at flange walls, taking into consideration the material properties of bars D4 used for the test.

openings. In that case, the measured stresses would not represent the actual stress conditions of the critical section of the wall. This would lead one to find that the stresses obtained as a product of the measured strain multiplied by elastic modulus were not reliable.

However, even if flexural cracks occurred at the bottom of the wall, where the moment becomes largest (critical section), the tensile forces might have been carried mainly by the steel bars. Therefore, the outcome of this research might not be so far from reality, and this is evidenced in the calculation of the effective reinforcement ratio because most of the reinforcement bars yielded at the critical section. The effects of cracks and yield hinge relocation should be carefully discussed and properly studied with the placement of other strain gauges attached to the concrete surface and steel bars along vertical axes in order to detect where cracks are disturbing the deformation readings. These considerations are to be taken up in future works.

6. Conclusions

Different crack patterns were observed among the different specimens studied. The specimen without the flange wall developed horizontal cracks in both directions at the bottom. The vertical reinforcement yielded, and concrete at the bottom showed compression failure. It can be said that the specimen was in flexural failure mode with ductile behavior. On the other hand, the specimen with the flange wall developed a large number of shear cracks, and, after the vertical reinforcement bars yielded, the strength decreased suddenly, showing brittle behavior.

Conventional methods of determining the ultimate flexural strength for RC walls yielded conservative prediction of the flexural strengths observed for the specimen without the flange wall. The same conventional methods underestimated the flexural ultimate strength for the specimen with the flange wall. It is considered that this underestimation is a consequence of a lack of knowledge of the mechanism that the wall develops at the flange walls and a lack of knowledge of the effective width considered for design.

The specimen with the flange wall showed a larger energy dissipation capacity than did the specimen without the flange wall.

The test results suggest that stress distribution at the wall in the out-of-plane direction was not uniform, and the stress distribution along flange walls did not follow a specific trend. It was therefore not possible to determine a specific value the effective flexural width from the results of the presented estimation.

This experimental study confirms that the effective width increases with imposed drift level. At a lateral drift of 1.52%, only the bars at the end of the flange did not yield.

It is still impossible to specify a single value for an effective flange width useful in all cases; but the underestimation of the effective width has been confirmed. Future testing must be performed to determine the behavior of RC walls with flange walls as boundary elements, in order to confirm the results of this test, and to study the behavior and response of these types of walls to combined actions. The combination of the axial and flexural behaviors should be included, and the dimensions of the wall should simulate continuous walls of more than one story. These walls should have a larger slenderness ratio than that presented in this test for the real scenario of RC walls in buildings to be reproduced.

Acknowledgements

This study was supported by the SATREPS project "Enhancement of Earthquake and Tsunami Mitigation Technology in Peru" with the collaboration of the training course of International Institute of Seismology and Earthquake Engineering, Building Research Institute.

References:

[1] S. Wood, J. Wight, and J. Moehle, "The 1985 Chile earthquake Observations on Earthquake Resistant construction in Viña del mar," A Report to the National Science Foundation Research grants ECE 86-03789, ECE 86-03264 and ECE 86-06089, Department of civil engineering university of Illinois at Urbana Champaign, Urbana, Illinois, February 1987.

[2] Architectural Institute of Japan, "Guidelines for Performance Evaluation of Earthquake Resistant Reinforced Concrete Buildings," 2005.

[3] American Concrete Institute, "Building Code Requirements for Structural Concrete and Commentary," ACI 318-08, 2008.

[4] European Committee for Standardization, "Eurocode 2: Design of Concrete Structures, Part 1: General Rules and Rules for Build-

ings," EN 1992-1-1:2004 (E), Revised final draft, Brussels, Belgium, December 2003.
[5] J. W. Wallace, "Evaluation of UBC-94 Provisions for Seismic Design of RC Structural Walls," Earthquake Spectra, Vol.12, No.2, pp. 327-348, May 1996.
[6] European Committee for Standardization, "Eurocode 8: Design of structures for earthquake resistance- Part 1: General Rules seismic actions and rules for buildings," EN 1998-1:2004 (E), Brussels, Belgium, December 2003.
[7] A. Shibata, "Dynamic Analysis of Earthquake Resistant Structures," Tohoku University Press, Sendai, 2010.

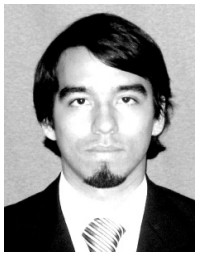

Name:
Sergio Sunley

Affiliation:
Visiting Staff, Universidad Centroamericana José Simeón Cañas

Address:
PO 01-168, San Salvador, El Salvador, Centro América

Brief Career:
2010- BSc Civil Engineer, Universidad Centroamericana José Simeón Cañas
2011- Master in Disaster Management (Earthquake Engineering group), IISEE, Building Research Institute, Japan
2012- Visiting Staff, Universidad Centroamericana José Simeón Cañas

Name:
Koichi Kusunoki

Affiliation:
Associate Professor, Yokohama National University

Address:
79-5 Tokiwadai, Hodogaya-ku, Yokohama, Kanagawa 240-8501, Japan

Brief Career:
2006-Associate Professor, Yokohama National University
2001-2006 Senior Researcher, Building Research Institute, Ministry of Construction
2000-2001 Researcher, Building Research Institute, Ministry of Construction

Selected Publications:
• K. Kusunoki, A. Tasai, and M. Teshigawara, "Development of building monitoring system to evaluate residual seismic capacity after an earthquake," 15th World Conference on Earthquake Engineering, 2012.9.
• K. Kabeyasawa and K. Kusunoki, "Damages to Reinforced Concrete Buildings Observed In Fukushima after the 2011 East Japan Earthquake," Proceedings of the International Symposium on Engineering Lessons Learned from the 2012 Great East Japan Earthquake, 2012.3.

Academic Societies & Scientific Organizations:
• Architectural Institute of Japan
• Japan Concrete Institute
• Japan Association for Earthquake Engineering

Name:
Taiki Saito

Affiliation:
Professor, Toyohashi University of Technology

Address:
1-1 Hibarigaoka, Tempaku-cho, Toyohashi 441-8580, Japan

Brief Career:
1990-1996 Research Associate, Tohoku University
1996-2000 Senior Research Engineer, Building Research Institute
2000-2012 Chief Research Engineer, Building Research Institute
2013- Professor, Toyohashi University of Technology

Selected Publications:
• T. Saito, T. Takahashi, R. Hasegawa, K. Morita, T. Azuhata, and K. Noguchi, "Shaking Table Test on Indoor Seismic Safety of High-rise Buildings (Part 2. Movement of Furniture under Long Period Earthquake Ground Motion," Proceedings of 14th World Conference of Earthquake Engineering, S10-014, 2008.10.

Academic Societies & Scientific Organizations:
• Architectural Institute of Japan (AIJ)
• Japan Association for Earthquake Engineering (JAEE)

Name:
Carlos Zavala

Affiliation:
Researcher, Laboratory of Structures, CISMID
Professor, Faculty of Civil Engineering, National University of Engineering

Address:
Los Ishipingos (Ex-Abetos) 245 Dpt. 202 Urb. El Remanso La Molina, Lima 12, Lima, Peru

Brief Career:
1984 Undergraduate Course, Faculty of Civil Engineering, National University of Engineering (UNI), Lima, Peru
1989 Master Course, Graduate School Faculty of Civil Engineering, National University of Engineering (UNI), Lima, Peru
1995 Ph.D., Graduate School of Architecture, University of Tokyo, Japan
2001 Professor, Faculty of Civil Engineering, National University of Engineering, Lima, Peru
2007-2012 Director of Japan Peru Center of Earthquake Engineering Research & Disaster Mitigation CISMID

Selected Publications:
• C. Zavala, K. Ohi, and K. Takanashi, "A general Scheme for Substructuring On-line Hybrid Test on Planar Moment Frames (The Neural Network Model)," Proceedings of 4th Pacific Steel Structures Conference, Pergamom Press, October 1995.
• C. Zavala, "Improvement on low cost housing through non-conventional construction systems," Proceedings of the 12th World Conference on Earthquake Engineering, Auckland, New Zealand, February 2000.
• C. Zavala, C. Honma, P. Gibu et. al, "Full Scale On Line Test On Two Story Masonry Building Using Handmade Bricks," Proceedings of the 13th World Conference on Earthquake Engineering (WCEE), Vancouver, Canada, August 2004.
• C. Zavala, Z. Aguilar, and M. Estrada, "Evaluation of SRSND Simulator against Fragility Curves for Pisco Quake," Proceedings of the 8th International Conference on Urban Earthquake Engineering Tokyo Institute of Technology, Tokyo, Japan, 2011.

Academic Societies & Scientific Organizations:
• Peru Engineering Association (CIP)